Remote Microwave Soil Drought Index Considering Dielectric Properties of Soil

Andrey N. Romanov, *Member, IEEE*, Ilya V. Khvostov, Ivan V. Ryabinin, Dmitry N. Troshkin, and Dmitry A. Romanov

***Abstract*— The article presents the innovative remote microwave soil drought index (RMSDI) developed for assessing intensity of soil drought (SD) and tested in the Kulunda arid steppe (West Siberia). RMSDI is based on satellite measurements of brightness and thermodynamic temperatures, including dependences of radio-emissivity on volume fraction of water (W) in soil calculated from soil dielectric characteristics. To define W and RMSDI, we employ the data on brightness temperatures obtained from soil moisture and ocean salinity (SMOS) and thermodynamic temperatures–from moderate resolution imaging spectroradiometer (MODIS). The territories falling within a SMOS pixel are major objects of our study (cell 4 010 458 discrete geodetic grid (DGG) icosahedral Snyder equal area (ISEA) 4H9). According to the MODIS data, the lakes and water source areas in a SMOS pixel makes up less than 0.1%. The total area of forest and water sources is insignificant (less than 0.1%). By granulometric composition, soils are referred to slit loam and loam ones. We offer the constructed for the test area graphs of seasonal dynamics of brightness and thermodynamic temperatures, radio-emissivity (χ), W, and RMSDI. Dependences of $W(\chi)$ are given for soils with different values of bound water (W_t). The established standardized dependence $\chi_t(W_t)$ makes it possible to express the value of χ_t via W_t. The satellite sensing data and dielectric characteristics of soils are used to calculate the values of W and RMSDI.**

***Index Terms*— Remote microwave sensing, soil drought (SD), soil moisture and ocean salinity (SMOS), soil volumetric moisture, West Siberia.**

I. Introduction

SOIL droughts (SDs) are hazardous natural phenomena, which occur at soil moisture (SM) content insufficient for normal plant growth. Regionally, these events differ in meteorological conditions, climate features, atmospheric circulation, and soil properties. Prolonged droughts, periodically observed worldwide in many agrarian regions, contribute to crop yield reduction that brings to rise in crop production costs.

Remote monitoring of SD is based on the laws of reflection, emissivity, and absorption of electromagnetic waves by soil and vegetation. To estimate SD, numerous remote indices in the optical range have been developed. However, their application is limited because of dependence on cloudiness, water vapor in the atmosphere, and precipitation [1], [2], [3], [4].

Manuscript received 1 March 2023; revised 25 April 2023, 28 May 2023, and 22 August 2023; accepted 7 September 2023. Date of publication 12 September 2023; date of current version 9 October 2023. This work was supported by the Russian Science Foundation under Grant 22-17-20041 (https://rscf.ru/project/22-17-20041/). *(Corresponding author: Andrey N. Romanov.)*

The authors are with the Institute for Water and Environmental Problems SB RAS, Barnaul 656038, Russia (e-mail: romanov_alt@mail.ru).

Digital Object Identifier 10.1109/TGRS.2023.3314463

To improve accuracy and reliability of optical remote monitoring methods, drought indices (DIs) are identified using sensitive to change SM remote data in the microwave range [5], [6]. SM is insufficiently informative though along with soil temperature it is the main parameter that quantitatively characterizes SD. For example, salt marshes and takyrs have high SM, but their vegetation cover is either extremely scarce or absent at all.

Remote indices based on the use of the AMSR-E data in cm and mm bands have become widespread [7], [8]. Surface roughness and dielectric constant of soil are taken into account in the advanced microwave scanning radiometer (AMSRE) L3 data-based monitoring of the Tibetan Plateau drought [9]. In order to monitor the drought process in China using the AMSR-E data [10], a remote index of drought (RID) based on the relationship between drought and changes in SM qualitatively reflecting drought development and its spread have been proposed. To calculate RID for the studied period, the minimum/maximum values of SM are chosen and compared with those of RID (from 0 to 100). In [11] and [12] the AMSR-E data and normalized multiband DI are used to obtain a combined SM. To monitor the strongest (over the past 100 years) drought in China (2009–2010), the microwave polarization index based on AMSR-E data [13] is employed.

In [14], different DI derived from the data of moderate resolution imaging spectroradiometer (MODIS), AMSR-E, etc., are compared. The findings suggest that in varying climate conditions these indices have their own strengths and weaknesses. For global monitoring of SM, the data of ASCAT installed on the METOP series satellites are used. The ASCAT data contribute to the real-time monitoring of droughts on a global scale, the identification of anomalies in SM and estimation of the drought severity index [15], [16]. Hernández-Sánchez et al. [17], present the relationship between the microwave polarization DI and the soil water deficit index using soil moisture active passive (SMAP) mission to define drought periods over a rainfed agricultural area. In [18] and [19], to reduce a pixel size, the SMAP data and the results of radar observations (sentinel-1) are used.

The standardized brightness temperatures (T_B) index based on the SM and ocean salinity (SMOS) data and distinguished by better spatial-temporal resolution is described in [20]. In [21], SM calculated from the SMOS data is compared with meteorological indices for drought monitoring in northeastern China. It is found that SM correlates with the standardized

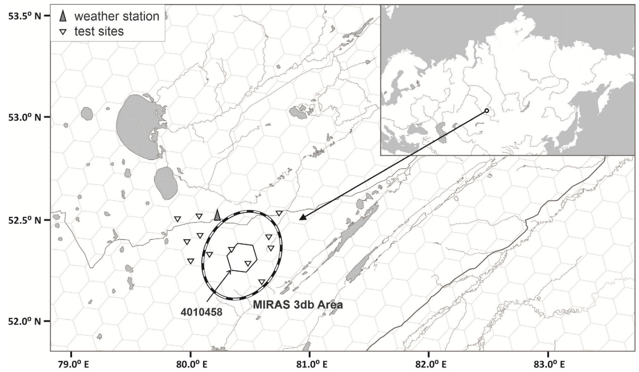

Fig. 1. Map of the study area: 4 010 458—the cell of DGG ISEA 4H9, black and white outline—a SMOS pixel.

precipitation index, the standardized precipitation and evapotranspiration index, and the SM anomaly percentage index. In [22], the improved DI based on passive microwave remote sensing (satellite FengYun) and optical/infrared data (MODIS) is proposed. This DI is a combination of the underlying surface T, SM and vegetation indices.

The SM water use efficiency index presented in [23] rests upon the use of SM data and normalized difference vegetation index (NDVI) for assessing susceptibility of an area to drought. NDVI is employed to identify the areas with low vegetation biomass. In Zhang et al. [24], describe the multiple remote sensing drought index based on remote sensing of SM, precipitation, and NDVI. The data on SM, precipitation, and land surface temperature are also used to calculate the microwave-integrated DI [25].

A remote method for determining drought due to T_B measurements (SMOS, AMSR-E/AMSR2) and estimations of water reserves according to the gravity recovery and climate experiment (GRACE) data is proposed in [26].

The SM anomaly percentage index is applied in monitoring of agricultural drought in India (2002–2014), as well as in spatiotemporal analysis of SM with the use of the AMSR-E (2002–2010) and SMOS (2010–2014) data [27], [28]. In [29], a review of microwave methods for remote monitoring of agricultural drought resting on the SMOS, SMAP, ASCAT, and AMRS-E data is presented; the main indicators of droughts taking into account SM are described. The shielding effect of vegetation cover on the underlying surface emissivity is considered. In [30], a review of DI is given. Interestingly, none of the existing indices can predict drought with high accuracy and reliability, especially in modern conditions of unpredictable climate change.

The main goal of our study is to develop a remote microwave soil drought index (RMSDI) taking into account emissivity characteristics of specific soils, as well as the phase composition and dielectric characteristics of SM.

II. Data and Methods

This article describes the developed RMSDI tested in Altai Krai. Field studies were carried out in the Kulunda steppe (KS) (Fig. 1).

The research methodology was discussed in detail in [31]. Here, seasonal dynamics of T_B (L1C) were studied in cell 4 010 460 discrete geodetic grid (DGG) ISEA 4H9 located to the north from cell 4 010 458 of the present work and characterized by different physical and dielectric properties of soil. The error range for the selected cells of DGG ISEA 4H9 (diameter: 16 km) and the test area (width: 300 km) was within ±3 K [32], [33].

The SMOS L1C dataset (MIR_SCLF1C products, versions 620 and 724) contained brightness temperatures correlated with the Earth surface radiation within individual cells of the ISEA 4H9 DGG and recorded by MIRAS antennas above the atmospheric surface at different incidence angles, as well as their values needed for further computational procedures (layers incidence_angle, azimuth_angle, geometric_rotation_angle, faraday_rotation_angle). The conversion of T_B values from the antenna-related coordinate system (BT_Value_X, BT_Value_H) to the surface-related one (BT_Value_H, BT_Value_V), the so-called "rotation" of the polarization vector, was performed using the SMOS-BOX package version 5.8.1 in the SNAP software environment. The description of this procedure was given in [33].

We used the SMOS L2SM dataset (MIR_SMUDP2 products, version 700) containing the soil_moisture layer (estimate of SM in soil layer) presented in [33]. From the analyzed data array we excluded: 1) values burdened by the influence of radio frequency interference (according to the quality flag RFI1); 2) values obtained outside the Alias Free (AF) region, free from overlapping image replicas (by the AF flag); 3) data with T_B errors exceeding 5 K; and 4) data with polarization coefficient ($T_{\mathrm{BH}}/T_{\mathrm{BV}}$) outside the range of 0.01–0.99.

For the regional monitoring of SD, satellite measurements of brightness (T_B) and thermodynamic (T) temperatures, field measurements of volume fraction of water (W) in soil, laboratory measurements of the refractive index (n) and the absorption factor (κ) were employed. The relationship between T_B and n, κ of soil was given in [34]. L1C SMOS [35] was involved in measuring T_B on horizontal polarization at angle of $\theta = 42.5°$. The L1C data were represented as DGG ISEA 4H9 [36] (Fig. 1). The linear cell size and area made up 16 km and 195 km^2; the longitudinal and transverse resolution of the L1C product–64 and 35 km, respectively.

Values of T were estimated from MOD11A1daily data available in the database LP DAAC (https://lpdaac.usgs.gov). This product contained values of T with a resolution of 1 km and a fixed measurement time [37]. Time difference between MODIS and MIRAS (SMOS) measurements did not exceed 2 h. The resolution of MIRAS (40 km^2) and MODIS (1 km^2) varied significantly. The MODIS data analysis showed minor (2 K) variations of T within each SMOS grid cell. Therefore, the MODIS product resolution can be lowered to the level of the SMOS data by means of data smoothing. To minimize differences between soil and vegetation temperatures, we used morning measurements when their temperatures were approximately the same.

The selected major sites fell into a MIRAS pixel (cell 4 010 458). The study area was a flat plain covered by stunt vegetation with negligible biomass. During the measurement period, vegetation suffered from insufficient moisture caused by drought. Lots of plants perished because of water deficit. According to the MODIS data, the lakes and water source areas in a SMOS pixel accounted for less than 0.1%. The total area of forest was also insignificant. According to the United States Department of Agriculture (USDA) classification, the study area was represented by silt loam and loam. In natural conditions, density (ρ), temperature (t), and volume fraction of water (W) in the surface soil layer (0–5 cm) varied as $\rho = 1.06$–1.35 g/cm^3; $\rho_{\text{dry}} = 1.05$–1.2 g/cm^3; $W = 0.05, \ldots, 0.28$ cm^3/cm^3; $t = 18, \ldots, 60$ °C.

The data of the long-term agrohydrological observations were evidence of weak SD recorded at $W \leq 0.08$ cm^3/cm^3, and severe drought–at $W \leq 0.055$ cm^3/cm^3. Biologically determined wilting point varied from 0.084 to 0.091 cm^3/cm^3 (at $\rho_{\text{wet}} = 1.08$–1.15 and $\rho_{\text{dry}} = 1.0$–1.07 g/cm^3).

According to [32], at remote sensing in the decimeter range from SMOS (1.4 GHz and low spatial resolution) of poorly-moistened soils of the dry steppe zone with a flat surface and low vegetation biomass, the following formula may suit:

$$T_B = \chi \cdot T_{\text{ef}} \tag{1}$$

where χ, T_{ef} are the emissivity and effective temperature of the skin layer of the underlying surface, $\chi = 4n/((n+1)^2 + \kappa^2)$. To establish experimental dependences $\chi(W)$, we measured n, κ of soils, $n + i\kappa = \sqrt{\varepsilon}$, $\varepsilon' = n^2 - \kappa^2$, $\varepsilon'' = 2n\kappa$ (ε', ε'' are the real and imaginary parts of complex permittivity ε).

On the soil surface, T depended on weather conditions and varied during the day from 298 to 333 K in summer. From the depth of 15–20 cm, T stabilized and changed within 296–298 K during the day. SMOS flew over the study area at 07:00 in the morning and at 20:00 in the evening local time. To perform an experiment, we selected the morning flyby data. By this time, T of the soil surface cooled down to 298–303 K. The experimentally established dependence $T(Z)$ has the form

$$T = 299.92 - 0.07378 \cdot Z, \quad 0 \leq Z \leq 70 \text{ cm}.$$

To calculate T_{ef}, we used the ratio derived for the study area

$$T_{\text{ef}} = T_0 - 0.07378/(0.13644 + 3.3354 \cdot W_Z) \tag{2}$$

where W_Z is the gradient W in the layer Z. In summer, the dependences W_Z have the form $W_Z = W_0 \pm A \cdot Z$, where $A = (2$–$6)\ 10^{-4}$ – the empirical coefficient depending on weather conditions.

This ratio was derived for the study (certain) territory for the morning soil temperature gradient. Note that its application to other hours and territories would require some adjustments. As follows from relation (2), any volumetric moisture in the skin layer is $L_{\text{ef}}\ \Delta T = (T_{\text{ef}}$–$T_0) < 1$ K.

To establish experimental dependences $\chi(W)$, we measured n, κ of soils. A detailed description of the laboratory setup and the technique of dielectric measurements was given in [38] and [39]. To measure dielectric properties, we used a bridge-type laboratory setup based on the FK2-18 phase-difference measuring device (Fig. 2) consisting of major elements: G—a high-frequency signal generator G4-78 (1.16–1.78 GHz), MPD—a matched power divider, LVL—a transmission line of variable length, A1, A2, A3—matching coaxial attenuators, I–a gauge unit of a phase meter, A—a reference channel, B—a measuring channel with a container (C) for the sample.

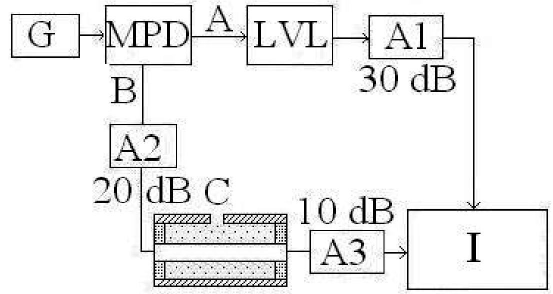

Fig. 2. Scheme of a bridge-type laboratory setup based on a phase-difference measuring device.

The container was configured as a coaxial waveguide. The signal produced by the generator was transferred to MPD and shared equally between the reference (A) and the measuring (B) channels. In the absence of the test specimen in the container, a zero value of the phase difference and amplitudes was set on the phase meter. Next, the tested sample was placed into the container; the phases and attenuation were measured by the phase-meter indicator.

To describe dc of samples, we applied the n and κ. Soil samples were placed in a completely filled measuring container (the brass coaxial waveguide of 37 mm long, with diameters of the outer shell and inner core of 16 and 7 mm, respectively) with further measuring the module and phase of complex transmittance of electromagnetic waves (1.41 GHz) through the tested specimen. A measurement resolution of the phase difference in signals (φ) made up 0.2°, attenuation (A) = 0.2 dB. Phase measurement errors $\Delta\varphi \leq (1 + 0.034\ \varphi_{\text{limit}} + 0{,}075$ A), attenuation $\Delta A \leq (0.5 + 0.02\ \text{A}_{\text{limit}} + 0.03$ A), where $\varphi_{\text{limit}} = 6°$, $A_{\text{limit}} = 3$ were limit values of the scales used.

The sources of probable measuring errors for dielectric and emissivity characteristics of soil may be: 1) inaccuracies in determining the specimen length; 2) incomplete filling of a waveguide container with specimens; and 3) variations in the density of different samples. It should be noted that a properly prepared specimen minimizes all the errors.

For a quantitative description of water contained in the samples, we used volume ($W = V_W/V$ [cm^3/cm^3]) and mass ($W_M = M_W\ /M$[g/g]) fractions related as: $W = (\rho_{\text{wet}}/\rho_w) \times W_M$, where V, V_W – the volumes of wet soil and water; $M = M_{\text{dry}} + M_W$, M, M_{dry}, M_W–the mass of wet, dry samples and water; ρ_{wet}, $\rho_W = 1$ [g/cm^3]–the densities of soil and water.

The equipment was calibrated before and after the measurements. On completing dielectric measurements, the sample was extracted from the container and weighed on analytical balance to the nearest 0.0001 g. To change W in the range $W > W_t$, a soil specimen was dehydrated at room temperature for 1–10 min, while at $W < W_1$ it was kept in a drying chamber at 105 °C.

Dielectric properties of soil were measured at gradual drying at W of 0.45–0.006 cm^3/cm^3. Before measuring, each sample was ground and thoroughly mixed till the unified condition. Depending on W and packing density in the measuring container, the mass of study samples made up 7–10 g, $\rho_{\text{wet}} = 1.2$–1.4 g/cm^3, $\rho_{\text{dry}} = 1.1$–1.3 g/cm^3.

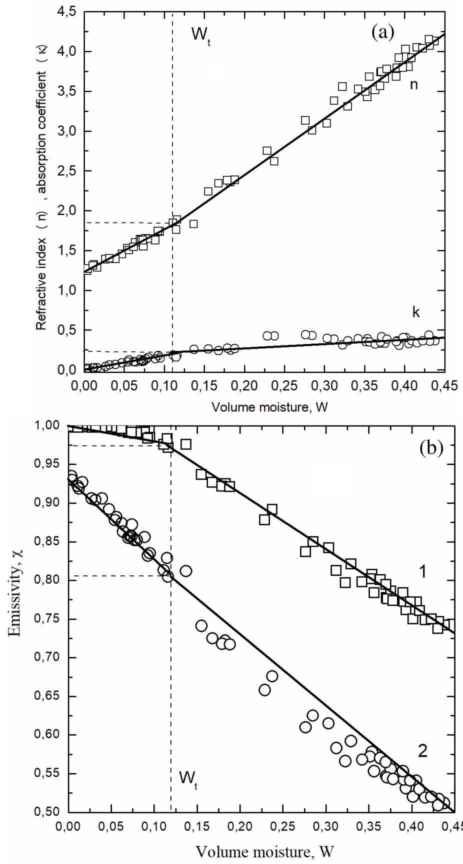

Fig. 3. Dependences of n, κ on W ($\rho_{\text{dry}} = 1.06$ g/cm^3). (a) and (b) Dependences of χ (1–v-polarization, 2–h-polarization) on W.

TABLE I

NUMERICAL VALUES OF n, κ FOR DIFFEREN W

n_0	n_t	n_w	κ_0	κ_t	κ_w
1.25	1.87	4.22	0.001	0.22	0.41

To validate satellite data, we collected soil samples at test sites and measured SM using the gravimetric method in laboratory conditions. The time difference between soil sampling and satellite flyby over the given territory did not exceed several hours. For comparison, we used the data obtained from the weather station.

III. RESULTS

For the study territory, the generalized dependence $(n,\ \kappa)(W)$ [Fig. 3(a)] was approximated by straight lines and calculated from the measured n, κ of soils falling into a MIRAS pixel. Dielectric measurements were carried out within the range $W = 0$–$W_{\max} = 0.45$ cm^3/cm^3. Two intervals of W with different behaviors of n and κ are distinguished on the graphs: 0–W_t and W_t–$W_{\max}$. $W_t = 0.11$ cm^3/cm^3 corresponds to the moisture content at the transition from bound to free water. Dielectric properties of bound and free water differ markedly [40], [41]. Table I represents values of n_0, κ_0 ($W = 0$, $\rho_{\text{dry}} = 1.06$ g/cm^3), n_t, κ_t ($W = W_t$), n_w, κ_w ($W = W_{\max}$) [derived from Fig. 3(a)]. Using the established relationships, the inverse dependence $W(\chi)$ can be represented

TABLE II

COMPLIANCE OF W AND RMSDI WITH A DEGREE OF MOISTURE USED IN AGROMETEOROLOGY

N	*W, [cm³/cm³]*	*RMSDI*	Moisture degree
1	0.000 – 0.026	-1.000 – -0.776	Severe soil drought
2	0.026 – 0.047	-0.776 – -0.595	Weak soil drought
3	0.047 – 0.08	-0.595 – -0.310	Insufficient hydration (strong)
4	0.08 – 0.112	-0.310 – -0.034	Insufficient hydration (weak)
5	0.112 – 0.16	-0.034 – 0.132	Optimum hydration
6	0.160 – 0.340	0.132 – 0.670	Excessive hydration
7	>0.34	>0.67	Swamping

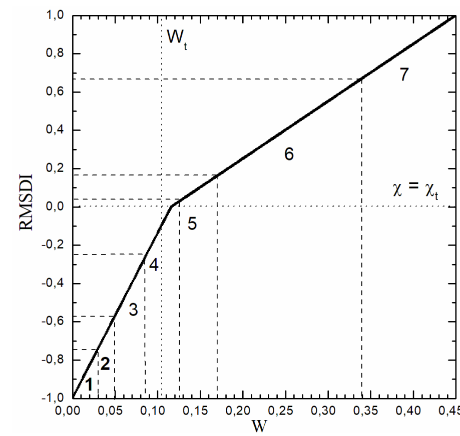

Fig. 4. RMSDI (W) dependence: 1–7–moisture degree (Table II).

as follows:

$$W = \begin{cases} A - B \cdot \chi, & \chi_t \le \chi \le \chi_0 \\ C - D\chi \cdot \chi, & \chi_w \le\le \chi_t. \end{cases} \tag{3}$$

For horizontal polarization and $\theta = 42.5°$, $\chi_0 = 0.94$; $\chi_t = 0.81$, $\chi_w = 0.50$ after simple transformations, let us write relation (3) in the standardized form

$$W = \begin{cases} W_t \dfrac{\chi_0 - \chi}{\chi_0 - \chi_t}, & \chi_t \le \chi \le \chi_0 \\ W_t + (W_{\max} - W_t)\dfrac{\chi_t - \chi}{\chi_t - \chi_w}, & \chi_w \le \chi \le \chi_t. \end{cases} \tag{4}$$

The value of χ_t can be obtained from simultaneous remote measurements of χ and field measurements of W, or from dielectric measurements of soil permittivity at different values of W. It is worth noting that field measurements of W are rather laborious; dielectric measurements require specialized equipment and software provision. In contrast to χ_t, the measurements of W_t are easily performed by most soil laboratories.

For a wide practical application of relations (3) and (4), we approximate $\chi_t(W_t)$ (h-polarization) with a linear dependence

$$\chi_t = 0.62521 - 0.69621 \cdot W_t, \quad \sigma = 0,0097, \ \ R = -0.97 \tag{5}$$

where R is the correlation coefficient, σ is the root mean square error.

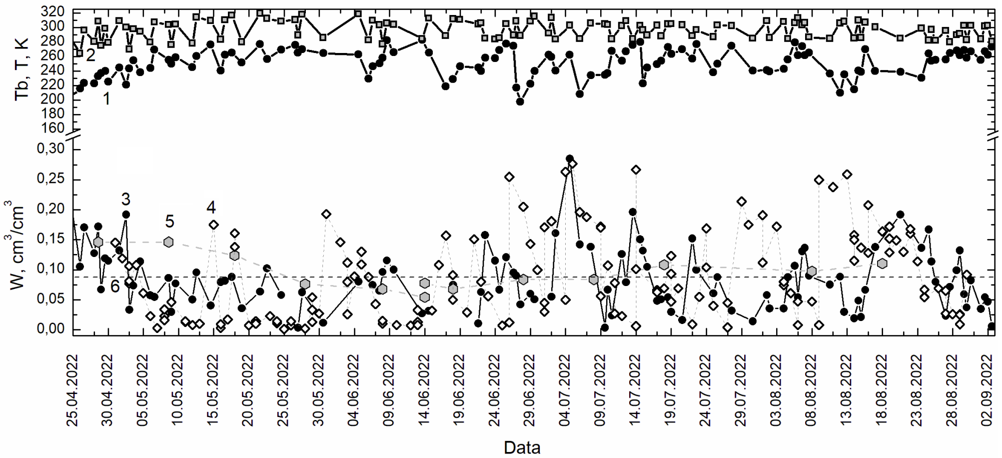

Fig. 5. Seasonal dynamic of T_B (1), T (2), W (3), algorithm SMOS (4), natural field measurements (5), wilting point (6).

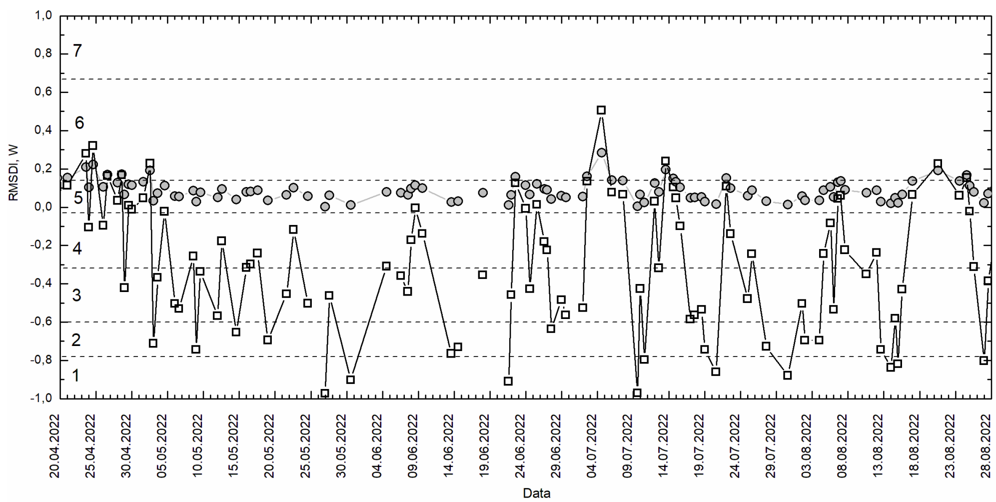

Fig. 6. Seasonal dynamics of W (circles), RMSDI (squares): 1–7–moisture degree (Table II).

SD occurs at $W \leq W_t$. In this case, only inaccessible (to plants) bound water is present in the soil. The value χ_t may serve as a radio-physical characteristic of SD. Values of χ correspond to the following regimes of SM: $\chi_t \leq \chi \leq \chi_0$– the lack of water in soil–drought; $\chi_w < \chi \leq \chi_t$ – the amount of water sufficient for plants. SD conditions are realized when $\chi_t \leq \chi$, reaching its maximum at $\chi \approx \chi_0$. To assess the degree of SM (including drought and waterlogging), we introduce the RMSDI as the ratio of interval lengths in different moisture ranges

$$\text{RMSDI} = \begin{cases} \dfrac{\chi_t - \chi}{\chi_0 - \chi_t}, & \chi_t \leq \chi \leq \chi_0 \\ \dfrac{\chi_t - \chi}{\chi_t - \chi_w}, & \chi_w \leq \chi \leq \chi_t. \end{cases}$$

The relation between RMSDI and W is

$$\text{RMSDI} = \begin{cases} (W/W_t - 1), & \chi_t \leq \chi \leq \chi_0 \\ (W - W_t)/(W_{\max} - W_t), & \chi_w \leq \chi \leq \chi_t. \end{cases}$$

Table II shows the numerical values of W and RMSDI corresponding to gradations of moisture degree of the territory used in agrometeorology. RMSDI (W) dependence is shown in Fig. 4.

Figs. 5 and 6 present graphs of seasonal dynamics of T_B, T, W, and RMSDI for the test site in 2022. Values of W and RMSDI were calculated from satellite measurements of T_B (SMOS) and T(MODIS) using (1) and (2). It can be seen that $W < W_t = 0.11$ cm^3/cm^3 for a significant part of the summer season. RMSDI proves the lack of SD in this area (Fig. 6).

In Fig. 6, dotted lines mark RMSDI intervals corresponding to different gradations of moisture degree. In this area, soil wetness (SW) is insufficient almost during the entire growing season, including the periods of weak and severe drought. Field measurements of W prove this fact (Fig. 5).

The error of remote determination of W depends on density, texture, salinity of soils, landscape diversity, and vegetation biomass. To estimate W, the L2SM SMOS algorithm is used with a declared error less than 0.04 cm^3/cm^3 [33]. From Fig. 6 it follows that in contrast to $W_{\text{NF,}}$ (natural field measurements), W_{SMOS} values show greater data scattering than W. In some cases, the discrepancy between W, W_{SMOS}, and W_{NF} can be associated with precipitation occurring during the time between the satellite and field measurements of W.

Generally, the application of the L2SM SMOS algorithm for estimating SM values suits researchers and end users.

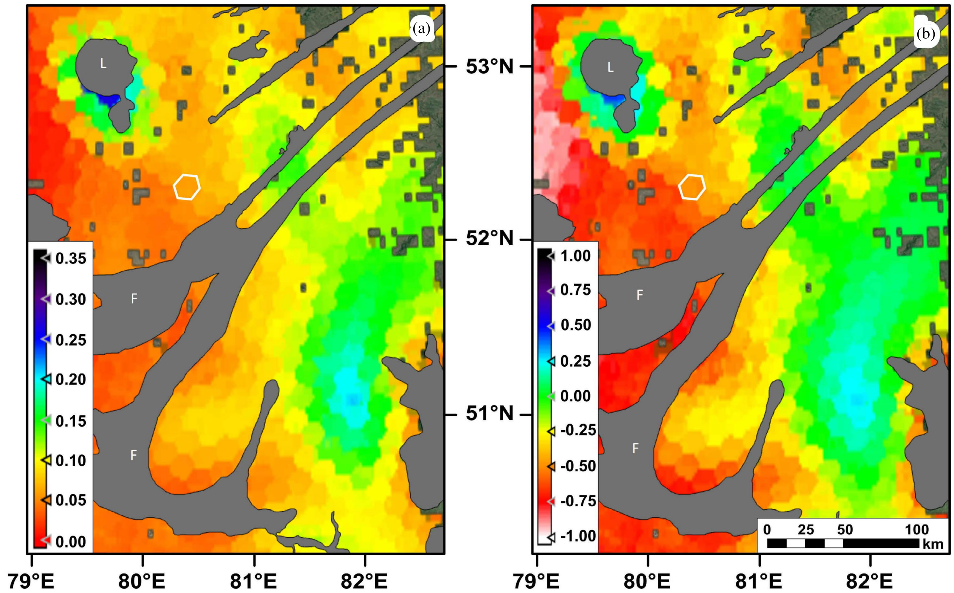

Fig. 7. Schematic maps of *W*. (a) RMSDI. (b) L–Lakes Kulundinskoye and Kuchuk; F–relict belt forests.

Unfortunately, in some cases, for solving practical problems and when dealing with specific sites of the Earth surface commensurate in area with the grid cell size, a satisfactory agreement between the values of Soil_Moisture of the MIR_SMUDP2 product and contact measurements of moisture in effectively radiating soil layer may be absent. For such special cases, adjustment of models and algorithms of SMOS is ill-advised. Therefore, the development of alternative algorithms based on the SMOS data of the first processing level ensuring a satisfactory result in the mentioned particular cases is still of interest.

Based on the results of satellite measurements of T_B, T, and dependences $W(\chi)$, we have constructed the schematic maps of spatial distribution of W and RMSDI (for $W_t = 0.11$) (Fig. 7).

Fig. 7 presents the schematic maps of spatial distribution of W and RMSDI for the territory in the south of West Siberia and Kazakhstan (June 19, 2022) in order to assess its moisture content and detect sites with a deficit of W. Though the drought index and SM are interrelated, they are intended for different tasks and purposes. The drought index expresses drought quantitatively according to the level of moisture gradation accepted in agrometeorology (Fig. 3). Unlike RMSDI, W is a characteristic of soil. The same W for soils with different W_t can be classified as drought and as waterlogging (for sand: $W_t = 0.02$, for silt: $W_t = 0.25$–0.30).

IV. Discussion

The algorithms for calculating W and RMSDI were tested in the landscape-homogeneous site. In this study, we did not pose the problem to consider landscape diversity (mosaicism) since this technique was well developed before.

The distinguishing feature of RMSDI is the use of dielectric measurements in calculations of χ_t and W_t, the microwave satellite data–in estimation of T_B and infrared–in T. To do that, we employ the SMOS L1C and MODIS data. The centimeter-range satellite data (AMSR-E, ASCAT, etc.) can be used to calculate RMSDI. In this case, the skin layer does not exceed 1–5 cm, in contrast to the decimeter range (SMOS, SMAP) where the skin layer can reach 15–20 cm (rooted soil layer). Since the surface soil layer (1–2 cm) in summer often contains less moisture than the underlying root one (15–20 cm), the use of T_B satellite data (in the centimeter range) and related calculated low values of SM can lead to misdiagnosis of drought.

An important factor for the widespread practical application of RMSDI is a feasible replacement of highly specific dielectric measurements of χ_t and W_t [Fig. 3(a) and (b)] by χ_t calculated from standard soil measurements W_t W_{wp} (wilting point) that ensures the data availability (to end users) required for calculating RMSDI.For any DI, it is important to determine the boundaries of its applicability. RMSDI tested in the arid areas demonstrates a good agreement with the data (own and from weather stations) on field measurements of W. As shown in Fig. 4 and Table II, RMSDI operating in the range $W = 0 - W_{\max}$ can also be used to detect waterlogged areas. At high values of W, the developed algorithm ensures the results close to W_{SMOS} and W_{NF} (Figs. 5 and 6). For the areas with high vegetation biomass (forest, shrubs, sunflower and corn crops), the necessity in using the algorithms [33] for data correction may arise.

The applicability of RMSDI to different soil types in different geographic areas has been not studied yet. The limited use of the developed algorithm can be associated with very low or very high values of W_t for stony, sandy ($W_t \leq 0.02$) and clay soils ($W_t \geq 0.30$).

V. Conclusion

Accuracy in remote identification of W is largely limited since different types of the underlying surface (water body, forest, soil) hit the radiometer pixel, the dimensions of which are smaller than its resolution.

In contrast to other similar indices, RMSDI qualitatively assesses drought with allowance made for dielectric properties of specific soils. A reliable use of RMSDI depends on the determined accuracy of dependencies $n(W)$, $\kappa(W)$, $\chi(W)$, χ_t, W_t.

The advantage of RMSDI is its ease of use: 1) RMSDI is calculated from the available SMOS and MODIS data; 2) evaluation of input parameters χ_0, χ_t, χ_w is implemented via the standard definition of ρ_{dry}, W_t; and 3) values of χ_w for different soils are within the error. Seasonal RMSDI-based analysis of the intensity and duration of droughts is feasible due to the satellite data accumulated for the period of study (the daily data is not strictly necessary).

References

[1] J. W. Rouse, R. H. Haas, J. A. Schell, and D. W. Deering, "Monitoring vegetation systems in the great plains with ERTS," in *Proc. 3rd ERTS Symp.*, 1973, pp. 309–317.

[2] Y. Sawada, T. Koike, E. Ikoma, and M. Kitsuregawa, "Monitoring and predicting agricultural droughts for a water-limited subcontinental region by integrating a land surface model and microwave remote sensing," *IEEE Trans. Geosci. Remote Sens.*, vol. 58, no. 1, pp. 14–33, Jan. 2020.

[3] J. D. Tarpley, S. R. Schneider, and R. L. Money, "Global vegetation indices from the NOAA-7 meteorological satellite," *J. Climate Appl. Meteorol.*, vol. 23, no. 3, pp. 491–494, Mar. 1984.

[4] F. N. Kogan, "Droughts of the late 1980s in the United States as derived from NOAA polar-orbiting satellite data," *Bull. Amer. Meteorolog. Soc.*, vol. 76, no. 5, pp. 655–668, May 1995.

[5] Y. Yao, X. Chen, and J. Qian, "Advance in agricultural drought monitoring using remote sensing data," *Spectrosc. spectral Anal.*, vol. 39, no. 4, pp. 1005–1012, Apr. 2019.

[6] M. Le Page and M. Zribi, "Analysis and predictability of drought in Northwest Africa using optical and microwave satellite remote sensing products," *Sci. Rep.*, vol. 9, no. 1, p. 1466, Feb. 2019.

[7] Z. Li, Y. Han, and T. Hao, "Assessing the consistency of remotely sensed multiple drought indices for monitoring drought phenomena in continental China," *IEEE Trans. Geosci. Remote Sens.*, vol. 58, no. 8, pp. 5490–5502, Aug. 2020.

[8] L. Liu et al., "The microwave temperature vegetation drought index (MTVDI) based on AMSR-E brightness temperatures for long-term drought assessment across China (2003–2010)," *Remote Sens. Environ.*, vol. 199, pp. 302–320, Sep. 2017.

[9] M. Qin, R. Zhong, and S. Wang, "Passive microwave remote sensing for soil moisture retrieval on Tibetan Plateau, China," in *Proc. 19th Int. Conf. Geoinformatic*, Jun. 2011, pp. 1–5.

[10] S. Wu and X. Zhu, "Using AMSR-E land product to monitor the drought process in China," in *Proc. IEEE Int. Geosci. Remote Sens. Symp.*, Jul. 2010, pp. 3894–3897.

[11] C.-F. Chen, M. C. Valdez, N.-B. Chang, L.-Y. Chang, and P.-Y. Yuan, "Monitoring spatiotemporal surface soil moisture variations during dry seasons in central America with multisensor cascade data fusion," *IEEE J. Sel. Topics Appl. Earth Observ. Remote Sens.*, vol. 7, no. 11, pp. 4340–4355, Nov. 2014.

[12] S. Park, J. Im, S. Park, and J. Rhee, "AMSR2 soil moisture downscaling using multisensor products through machine learning approach," in *Proc. IEEE Int. Geosci. Remote Sens. Symp. (IGARSS)*, Milan, Italy, Jul. 2015, pp. 1984–1987.

[13] K. B. Mao, C. Y. Gao, L. J. Han, W. Zhang, and H. J. Tang, "The drought monitoring in China by using AMSR-E data," in *Proc. 2nd IITA Int. Conf. Geosci. Remote Sens.*, vol. 1, Aug. 2010, pp. 181–184.

[14] L. Zhang, W. Jiao, H. Zhang, C. Huang, and Q. Tong, "Studying drought phenomena in the continental United States in 2011 and 2012 using various drought indices," *Remote Sens. Environ.*, vol. 190, pp. 96–106, Mar. 2017.

[15] L. Brocca et al., "A review of the applications of ASCAT soil moisture products," *IEEE J. Sel. Topics Appl. Earth Observ. Remote Sens.*, vol. 10, no. 5, pp. 2285–2306, May 2017.

[16] W. Wagner et al., "The ASCAT soil moisture product: A review of its specifications, validation results, and emerging applications," *Meteorologische Zeitschrift*, vol. 22, no. 1, pp. 5–33, Feb. 2013.

[17] J. C. Hernández-Sánchez et al., "Identification of drought periods in agricultural areas using enhanced SMAP brightness temperature product," in *Proc. IEEE Int. Geosci. Remote Sens. Symp.*, Jul. 2021, pp. 1522–1525.

[18] Z. Wu, J. Qiu, W. T. Crow, D. Wang, Z. Wang, and X. Zhang, "Investigating the efficacy of the SMAP downscaled soil moisture product for drought monitoring based on information theory," *IEEE J. Sel. Topics Appl. Earth Observ. Remote Sens.*, vol. 15, pp. 1604–1616, 2022.

[19] Y. Huang, J. P. Walker, Y. Gao, X. Wu, and A. Monerris, "Estimation of vegetation water content from the radar vegetation index at L-band," *IEEE Trans. Geosci. Remote Sens.*, vol. 54, no. 2, pp. 981–989, Feb. 2016.

[20] Y. H. Kerr et al., "The SMOS mission: New tool for monitoring key elements of the global water cycle," *Proc. IEEE*, vol. 98, no. 5, pp. 666–687, May 2010.

[21] T. Cheng, S. Hong, B. Huang, J. Qiu, B. Zhao, and C. Tan, "Passive microwave remote sensing soil moisture data in agricultural drought monitoring: Application in northeastern China," *Water*, vol. 13, no. 19, p. 2777, Oct. 2021.

[22] Z. Wang, P. Guo, and H. Wan, "Improved drought monitoring method based on multisource remote sensing data," in *Proc. IEEE Int. Geosci. Remote Sens. Symp.*, Sep. 2020, pp. 5282–5285.

[23] S. Kang, N. Do, and S. Hong, "Assessing drought vulnerability using soil moisture-based water use efficiency in Northeast Asia dryland regions," in *Proc. IEEE Int. Geosci. Remote Sens. Symp. (IGARSS)*, Jul. 2016, pp. 5209–5212.

[24] Q. Zhang, R. Shi, C.-Y. Xu, P. Sun, H. Yu, and J. Zhao, "Multisource data-based integrated drought monitoring index: Model development and application," *J. Hydrol.*, vol. 615, Dec. 2022, Art. no. 128644.

[25] H. Laachrate, A. Fadil, and A. Ghafiri, "Drought monitoring of some Moroccan agricultural areas: Settat and Meknes using remote sensing techniques and a soil moisture-based drought index," in *Proc. IEEE Int. Conf. Moroccan Geomatics (Morgeo)*, May 2020, pp. 1–5.

[26] W. Chen, C. Huang, and Z.-L. Yang, "More severe drought detected by the assimilation of brightness temperature and terrestrial water storage anomalies in Texas during 2010–2013," *J. Hydrol.*, vol. 603, Dec. 2021, Art. no. 126802.

[27] P. Thiruvengadam and Y. S. Rao, "Spatio-temporal variation of soil moisture and drought monitoring using passive microwave remote sensing," in *Proc. IEEE Int. Geosci. Remote Sens. Symp. (IGARSS)*, Jul. 2016, pp. 3126–3129.

[28] Z. Y. Wu, G. H. Lu, L. Wen, and C. A. Lin, "Reconstructing and analyzing China's fifty-nine year (1951–2009) drought history using hydrological model simulation," *Hydrol. Earth Syst. Sci.*, vol. 15, no. 9, pp. 2881–2894, Sep. 2011.

[29] M. Vreugdenhil et al., "Microwave remote sensing for agricultural drought monitoring: Recent developments and challenges," *Frontiers Water*, vol. 4, Nov. 2022, Art. no. 1045451.

[30] Y. Yihdego, B. Vaheddoost, and R. A. Al-Weshah, "Drought indices and indicators revisited," *Arabian J. Geosci.*, vol. 12, no. 3, p. 69, Feb. 2019.

[31] A. Romanov, I. Ryabinin, I. Khvostov, D. Troshkin, and D. Romanov, "Remote radio-physical harbingers of drought in steppes of the south of Western Siberia," *Remote Sens.*, vol. 14, no. 23, p. 6141, Dec. 2022.

[32] Y. H. Kerr et al., "The SMOS soil moisture retrieval algorithm," *IEEE Trans. Geosci. Remote Sens.*, vol. 50, no. 5, pp. 1384–1403, May 2012.

[33] *Algorithm Theoretical Basis Document (ATBD) for the SMOS Level 2 Soil Moisture Processor Development Continuation Project*, document SO-TN-ARG-L2PP-0037, Sep. 2019.

[34] F. T. Ulaby, R. K. Moore, and A. K. Fung, *Microwave Remote Sensing Active and Passive: From Theory to Applications*. Norwood, MA, USA: Artech House, 1986.

[35] A. Gutierrez, R. Castro, P. Vieira, G. Lopes, J. Barbosa "SMOS L1 processor L1c data processing model," Tech. Rep. SO-DS-DME-L1OP-0009, Nov. 2017.

[36] K. Sahr, D. White, and A. J. Kimerling, "Geodesic discrete global grid systems," *Cartography Geographic Inf. Sci.*, vol. 30, no. 2, pp. 121–134, Jan. 2003.

[37] Z. Wan, "MODIS land-surface temperature algorithm theoretical background document (LST ATBD)," Version 3.3, Tech. Rep. NAS5-31370, Apr. 1999. [Online]. Available: https://doi.org/10.5067/MODIS/MYD11A1.061

[38] A. N. Romanov, "Some behavior features of dielectric properties of water in birch wood at a frequency of 1.41 GHz," *IEEE Trans. Geosci. Remote Sens.*, vol. 60, 2022, Art. no. 4409208, doi: 10.1109/TGRS.2022.3157642.

[39] A. N. Romanov, "Dielectric properties of water in saline soil and its solonchak vegetation at a frequency of 1.41 GHz," *IEEE Geosci. Remote Sens. Lett.*, vol. 18, no. 12, pp. 2033–2037, Dec. 2021, doi: 10.1109/LGRS.2020.3014374.

[40] J. R. Wang and T. J. Schmugge, "An empirical model for the complex dielectric permittivity of soils as a function of water content," *IEEE Trans. Geosci. Remote Sens.*, vol. GE-18, no. 4, pp. 288–295, Oct. 1980.

[41] M. Dobson, F. Ulaby, M. Hallikainen, and M. El-Rayes, "Microwave dielectric behavior of wet soil—Part II: Dielectric mixing models," *IEEE Trans. Geosci. Remote Sens.*, vol. GE-23, no. 1, pp. 35–46, Jan. 1985.

Andrey N. Romanov (Member, IEEE) received the bachelor's degree from the Faculty of Physics, Altai State University, Barnaul, Russia, in 1986, the Ph.D. degree from Altai State University, in 1994, and the Doctoral degree from IWEP SB RAS, Barnaul, in 2005.

His research interests include dielectric and emission characteristics of frozen and salted soils, water solutions, and microwave remote sensing of Earth covers.

Ilya V. Khvostov received the bachelor's degree from the Faculty of Physics and Technology, Altai State University, Barnaul, Russia, in 2004, with focus on radiophysics and geoinformatics, and the Ph.D. degree in 2007.

He has experience in analyzing satellite data at all levels of processing using both standard and proprietary algorithms.

Ivan V. Ryabinin received the bachelor's degree from the Faculty of Physics and Technology, Altai State University, Barnaul, Russia, in 2010, and the master's degree from Altai State University, in 2012.

His research interests include the development of methods for remote sensing of the underlying surface using satellite data.

Dmitry N. Troshkin received the bachelor's degree from the Faculty of Physics, Altai State University, Barnaul, Russia, in 1997, with focus on atmospheric physics and remote sensing, and the Ph.D. from Nagoya University, Nagoya, Japan, in 2003.

From 2003 to 2005, he held a Post-Doctoral position at Nagoya University, and Kanazawa University, Kanazawa, Japan. His research interests include the analysis of remote sensing data.

Dmitry A. Romanov received the bachelor's degree from the Faculty of Physics, Novosibirsk State University, Novosibirsk, Russia, in 2019, and the master's degree from Novosibirsk State University, in 2021.

His research interests include radiophysics, radio electronics, remote sensing, development of autonomous systems for monitoring the underlying surface, and programming.